DIELECTRIC-LOADED ANTENNAS

A transmit antenna converts the energy of a guided wave in a transmission line into the radiated wave in an unbounded medium. The receive antenna does the reverse. The transmission lines such as waveguides, coaxial lines, and microstrip lines use conductors mostly to confine and guide the energy, but antennas use them to radiate it. Because the radiated energy is in an unbounded region, phase control is often used to direct the radiation in the desired direction. Dielectrics play an important role in this process, and this article discusses a few representative cases. An important antenna parameter is its directivity, which is the measure of its control over the energy flow. To increase the directivity the antenna size must be increased, and the influence of dielectrics on their performance changes considerably. Thus, in this article, the use of dielectrics in antenna applications is divided into two categories: large high-gain antenna applications and small low-gain antenna applications.

In high-gain antenna applications, reflectors and lenses are used extensively (1). They operate principally on the basis of their geometry. Consequently, they are relatively low cost, reliable, and wideband. Reflectors are usually made of good conductors, and thus have lower loss, and because of their

high strength they can be made light. However, reflectors suffer from limited scan capability. Lenses, on the other hand, because of transparency, have more degrees of freedom—that is, two reflecting surfaces and the relative permittivity or refractive index. They also do not suffer from aperture blockage. However, lenses have disadvantages in large volume and weight.

In microwave antenna applications, lenses have numerous and diverse applications, but in most cases they are large with respect to the wavelength. Thus, physical and geometrical optics apply, and most of the lens design techniques can be adopted from optics to microwave applications. The aperture theory and synthesis techniques can also be used effectively to facilitate designs. In addition, the use of optical ray path in lens design makes the solution frequency-independent. In practice, however, the lens size in microwave frequencies is finite with respect to the wavelength, and the feed antenna is frequency-sensitive. Thus, the performance of the lens antenna also becomes frequency-dependent.

Natural dielectrics at microwave frequencies have reflective indices larger than unity, and for collimation they need convex surfaces. However, artificial media using guiding structures, such as waveguides, are equivalent to dielectrics with refractive index less than unity, and they result in concave lenses. They are usually dispersive, resulting in variation of the refractive index with frequency, and have narrower operating bandwidths.

In small antennas, dielectrics are used often to improve the radiation efficiency and polarization of other antennas, such as waveguides and horns. This is important in telecommunication applications where polarization control is required to implement frequency reuse and minimize interference, especially in satellite and wireless communications. Horn antennas and reflector feeds are examples that incorporate dielectrics or lens loading to improve performance (2).

Another area of important dielectric use is insulated antennas, in biological applications and remote sensing with buried or submerged antennas. The use of dielectric loading eliminates direct radio-frequency (RF) energy leak into the lossy environments, and it ensures radiative coupling into the target objects. Often a full wave analysis is needed to provide a proper understanding of resonance property and coupling mechanism to the surrounding media.

Finally, the antenna miniaturization depends primarily on the dielectric loading. Low-loss dielectrics with medium to high relative permittivities are now available and are used increasingly to reduce the antenna size. A number of important areas include dielectric-loaded waveguides and horns, dielectric resonator antennas, and microstrip antennas. By aperture loading of waveguides and small horns, excellent pattern symmetry and low cross-polarization can be obtained, which are essential features of reflector and lens feeds. In addition, the dielectric loading reduces their size and makes them useful candidates for multiple beam applications, using reflectors and lenses. Miniaturization of the antenna is also an important requirement in wireless communications. Microstrip patch or slot antennas with high relative permittivity substrates play an important role in this area, and their derivatives are used in most applications.

DIELECTRIC LENS ANTENNAS

In optical terms a lens produces an image of a source point at the image point. These points could be located anywhere
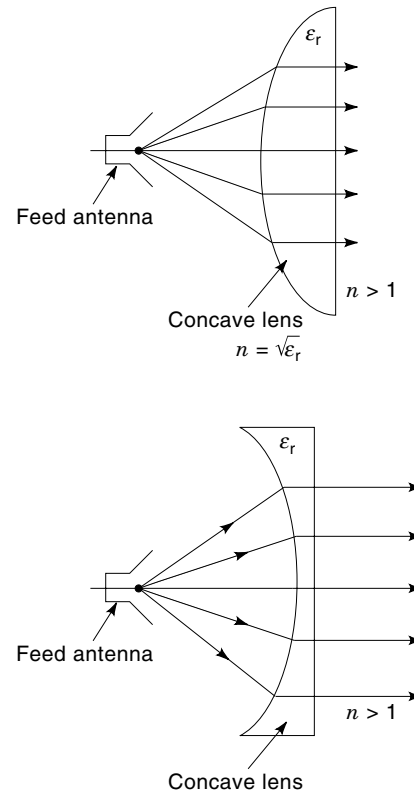

Figure 1. Geometry of lens antennas.

in space. For an antenna, this property means that the source and image points are focused at each other and the lens has two focal points. In turn, these focal points signify locations in space, where rays emanating from the lens arrive at equal phases. This property provides a mathematical relationship for describing the lens operation and, hence, its design.

To simplify the mathematics, the lens configuration is assumed to be rotationally symmetric, and the focal points are placed on its axis. A further simplification can be made for antenna applications, where the image point moves to infinity. That is, the lens focuses a nearby source point, on its axis, to another axial point at infinity. In such a case, all rays leaving the lens travel parallel to its axis, and their phase fronts are planes normal to the lens axis. This is shown in Fig. 1, where ϵ_r is the relative permittivity of the lens material and $n = \sqrt{\epsilon_r}$ is its refractive index.

To design the lens, one needs to determine the geometry of its two faces, front and back, or the coordinates x_1, y_1, and x_2, y_2 of points P_1 and P_2 (Fig. 2). There are four unknowns to be determined. The equality of the phase on the phase fronts requires that the electrical length between the focal points and the phase fronts be independent of the path lengths. This provides one equation. Two other equations can be obtained from the ray optics at the lens interface points P_1 and P_2, namely, Fermat's principle of minimum path lengths. This enforces the well-known Snell's law of refraction at the lens surface points. An additional relationship must be generated from the required lens properties, to enable a unique solution for the lens design.

To enforce the invariance of the ray path length, the central ray passing through points A, B, and C is selected as the
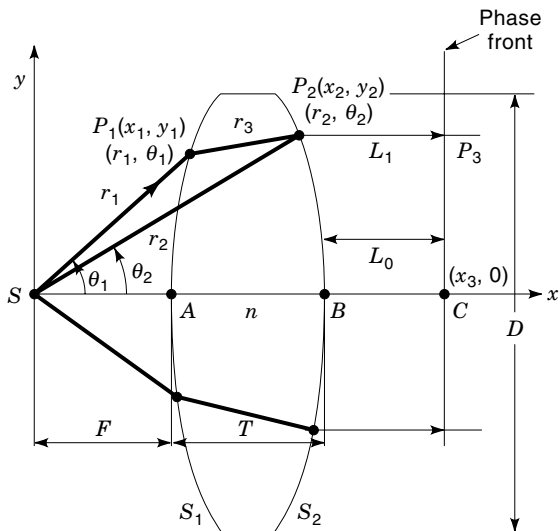
Figure 2. Geometry of a lens indicating ray and surface coordinates.

reference, and its length from S to C is compared with that of the ray passing through points P_1, P_2, and P_3. This provides the following equation:

$$\overline{SP_1} + n\overline{P_1P_2} + \overline{P_2P_3} = \overline{SA} + n\overline{AB} + \overline{BC} \qquad (1)$$

or

$$r_1 + nr_3 + L_1 = F + nT + L_0 \qquad (2)$$

where in terms of P_1 and P_2 coordinates each length is given by

$$
\begin{aligned}
r_1 &= (x_1^2 + y_1^2)^{1/2} \\
r_3 &= [(x_2 - x_1)^2 + (y_2 - y_1)^2]^{1/2} \\
L_1 &= (x_3 - x_2) \\
L_0 &= x_3 - (F + T)
\end{aligned}
\qquad (3)
$$

and F and T are the lens focal length and axial thickness and are therefore constant lengths defining the lens.

Enforcing Fermat's principle at points P_1 and P_2 results in differentiation of the path length in Eq. (1) in terms of its variables x_1, y_1 and x_2, y_2 and setting it to zero. This provides the slope of the lens surface profiles at each point P_1 and P_2.

At point P_1, one obtains

$$\frac{d}{dx_1}[r_1 + nr_3 + L_1] = \frac{d}{dx_1}[F + nT + L_0] = \frac{d}{dx_1}L_0 \qquad (4)$$

where F and T are constants. After simplification, one obtains

$$\frac{dy_1}{dx_1} = \frac{x_1 r_3 - (x_2 - x_1)\,nr_1}{(y_2 - y_1)\,nr_1 - y_1 r_3} \qquad (5)$$

At point P_2, a similar differentiation in terms of x_2 gives

$$\frac{dy_2}{dx_2} = \frac{(x_2 - x_1)n - r_3}{(y_2 - y_1)n} \qquad (6)$$

Equations (2), (5), and (6) are three fundamental equations used to design the required lens. Without another relationship, x_1 may be selected as the independent variable. Then others (i.e, x_2, y_1, and y_2) become dependent variables to be determined in terms of x_1. The solutions give the lens profiles in rectangular coordinates. If the lens profiles in polar coordinates are required, Eqs. (2), (5) and (6) can be obtained in terms of r_1, θ_1, and r_2, θ_2, the polar coordinates of P_1 and P_2. Differentiating Eqs. (2) in terms of θ_1 and θ_2 gives

$$\frac{dr_1}{d\theta_1} = \frac{nr_1r_2\sin(\theta_2 - \theta_1)}{r_3 - n[r_2\cos(\theta_2 - \theta_1) - r_1]} \qquad (7)$$

and

$$\frac{dr_2}{d\theta_2} = \frac{nr_1r_2\sin(\theta_2 - \theta_1) + r_2r_3\sin\theta_2}{r_3\sin\theta_2 - n[r_2 - r_1\cos(\theta_2 - \theta_1)]} \qquad (8)$$

where use is made of the following polar coordinate relationships:

$$
\begin{aligned}
x_1 &= r_1\cos\theta_1 \\
y_1 &= r_1\sin\theta_1 \\
x_2 &= r_2\cos\theta_2 \\
y_2 &= r_2\sin\theta_2 \\
r_3 &= |r_1 - r_2| = [r_1^2 + r_2^2 - 2r_1r_2\cos(\theta_2 - \theta_1)]^{1/2}
\end{aligned}
\qquad (9)
$$

Solutions of Eqs. (7) and (8) give the lens profiles in polar coordinates, which are often more compact in form. Also, for some simple lens configurations they result in well-known and easily recognizable parametric equations of the conic sections, generalizing the solution.

Examples, Simple Lenses

The lens design becomes considerably easier if one of its surfaces is predetermined. This eliminates one of the differential equations, as the surface profile is already known. The planar and spherical surfaces are among the simpler surfaces to select. The planar surfaces are normal to the lens axis. Such selections give simple profile equations. The planar surface is described by a constant x coordinate, and the spherical one is described by a constant polar coordinate r. These simplifications also assist in solutions of the other lens profile, for which an analytic solution can also be determined. Since either of the lens profiles can be predetermined as planar or spherical, four possible solutions exist. Only two, however, result in simple conical sections.

If the second surface S_2 is assumed to be planar and normal to the lens axis, the rays arriving from the right-hand side, parallel to the lens axis x, enter the lens unaffected and change direction only after the first lens surface S_1. Then they focus at S. That is, only the S_1 surface of the lens collimates the beam. Looking from the left side, spherical rays originating from the focal point S enter the lens S_1 and become parallel to its axis. Thus, after leaving the lens at S_2, since they are normal to S_2, their direction remains unchanged. In this case, the active surface S_1 of the lens is a hyperbola in a cylindrical lens but is hyperboloid in a rotationally symmetric lens.

If the surface S_1 is spherical, it becomes inactive, since the focal point is a point source and rays emanating from it constitute spherical waves. Thus, when S_1 is predetermined as a
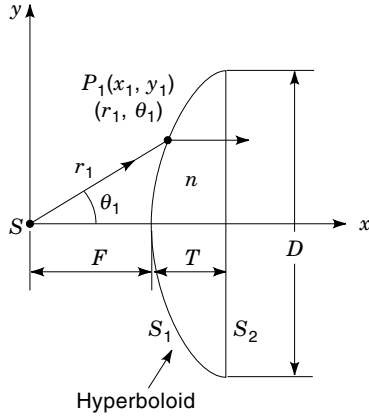
Figure 3. Geometry of lens with a planar surface S_2.

spherical surface, they enter the lens unaffected. Their collimation is done entirely by the lens's second surface S_2. Its surface is again a conic section and its cross section is elliptic. In the other two cases, both surfaces S_1 and S_2 of the lens participate in beam collimation and consequently are enter-dependent and more complex.

Lens with Planar S_2. On S_2, x is constant and slope is infinite (Fig. 3), and the surface is defined by

$$x_2 = F + T$$
$$y_2 = y_1 \tag{10}$$

A consequence of this is $L_1 = L_0$ in Eq. (2); when we use Eqs. (10), Eq. (2) becomes

$$r_1 + nr_3 = F \tag{11}$$

which, when using Eq. (10), becomes a function of x_1 and y_1. It can be solved directly to yield the profile of S_1 as

$$y_1^2 - (n^2 - 1)(x_1 - F)^2 = 2(n - 1)F(x_1 - F) \tag{12}$$

or, in polar coordinates,

$$r_1 = \frac{(n-1)F}{n\cos\theta_1 - 1} \tag{13}$$

They represent rectangular and polar equations of a hyperbola, which is the lens profile on S_1. They can be used also to determine the lens thickness on the axis. For this, one can use two extreme rays passing through its tip and the axis. The equality of the electrical lengths gives

$$F + nT = r_1(\theta_{1\max}) = \left[\left(\frac{D}{2}\right)^2 + (F + T)^2 \right]^{1/2} \tag{14}$$

A solution of this equation gives the lens thickness T as

$$T = (n + 1)^{-1} \left[\left(\frac{(n+1)D^2}{4(n-1)} + F^2 \right)^{1/2} - F \right] \tag{15}$$

and

$$\begin{aligned} \theta_{1\max} &= \cos^{-1}\left(\frac{1}{n}\right) \\ &= \tan^{-1}\left[\left(\frac{D}{2}\right) \Big/ (F + T) \right] \end{aligned} \tag{16}$$

Equation (16) shows that, for a given dielectric, the lens aperture angular size is limited by its refractive index n. In other words, with common dielectrics there is a limit on the compactness of the lens. That is, the focal length F cannot be reduced beyond the limit specified by Eq. (16).

Lens with Planar S_1. In this case, both lens surfaces contribute to the beam collimation. Its surface can be determined similar to case (a) by enforcing $x_1 = F$ and infinite slope for S_1 (Fig. 4). The results are (3)

$$x_1 = F$$

$$x_2 = \frac{\{[(n-1)T - [F^2 + y_1^2]^{1/2}][(n^2 - 1)y_1^2 + n^2 F^2]^{1/2} + n^2 F[F^2 + y_1^2]^{1/2}\}}{[n^2(F^2 + y_1^2)^{1/2} - [(n^2 - 1)y_1^2 + n^2 F^2]^{1/2}]}$$

$$y_2 = y_1 \left[1 + \frac{(x_2 - F)}{[(n^2 - 1)y_1^2 + n^2 F^2]^{1/2}} \right]$$

$$T = \frac{1}{2}(n - 1)^{-1}[(4F^2 + D^2)^{1/2} - 2F] \tag{17}$$

Note that since the beam collimation is due to both surfaces, the coordinates of S_2 are now dependent on those of S_1.

Lens with One Spherical Surface. When S_1 is a spherical surface, all spherical waves originating at the focal point S pass through it unaffected. The second surface S_2 collimates the beam. The geometry is shown in Fig. 5, and S_2 is an ellipse given

$$r_2 = \frac{(n-1)R}{n - \cos\theta_2} \tag{18}$$

where $R = F + T$ and other parameters are defined in Fig. 5. Its equation in rectangular coordinates has the form

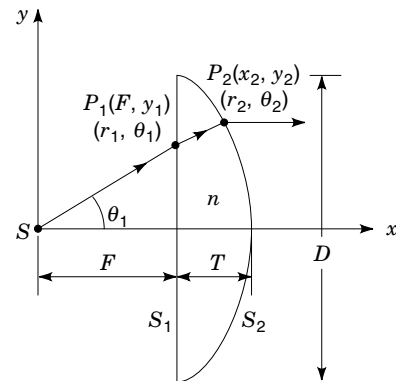$$y_2 = \left[\left[\frac{x_2 + (n-1)R}{n} \right]^2 - x_2 \right]^{1/2}$$

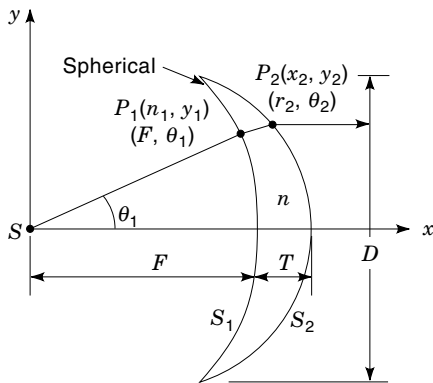**Figure 4.** Geometry of lens with a planar surface S_1.

Figure 5. Geometry of lens with a spherical surface S_1.

and

$$T = \frac{1}{2}(n-1)^{-1}[2F - (4F^2 - D^4)^{1/2}]$$

$$\theta_{2\,max} = \cos^{-1}\left(\frac{1}{n}\right) \tag{19}$$

The last equation again sets a limit for the peak angular aperture of the lens for a given dielectric material.

When the surface S_2 is assumed spherical, then both lens surfaces participate in collimating the beam. The inner surface S_1 can be obtained from (3)

$$n^2[r_2^2 + r_1^2 - 2r_1r_2\cos(\theta_1 - \theta_2)] = [(n-1)T + r_2\cos\theta_2 - r_1]^2$$

$$n^2 r_1 \sin(\theta_1 - \theta_2) = \sin\theta_2[(n-1)T + r_2\cos\theta_2 - r_1]$$

$$T = \left[\frac{4(n-1)F^2 - (n-3)D^2}{4(n-1)(n-3)^2}\right]^{1/2} + \frac{F}{n-3} \tag{20}$$

EFFECT OF LENS ON AMPLITUDE DISTRIBUTION

The lens equations, Eqs. (1) to (6), were based on the ray path analysis, or in antenna terms the phase relationships. The amplitude distributions were not considered. In practical applications, however, the amplitude distributions are also important and will influence the aperture efficiency of the lens, sidelobe levels, and cross-polarization. To state it briefly, a uniform aperture distribution gives the highest directivity, but has high sidelobes because of its high edge illumination. Sidelobes can be reduced by tapering the field toward the edge. Excessive tapering, however, rapidly reduces the lens directivity. It is therefore useful to know the influence of the lens on the field amplitude as well.

Assume that $A(\theta)$ is the angular dependence of the wave amplitude radiating from the focal points; and assume that $A(\rho)$, with $\rho = r\sin\theta$, is the amplitude distribution of the collimated beam. Then, using the conservation of power and neglecting the reflection at the lens surface, the following amplitude relationships can be obtained (1).

Hyperbolic lens with planar S_2

$$\frac{A(\rho)}{A(\theta_1)} = \frac{1}{F}\left[\frac{(n\cos\theta_1 - 1)^3}{(n-1)^2(n - \cos\theta_1)}\right]^{1/2} \tag{21}$$

Elliptic lense with spherical surface S_1

$$\frac{A(\rho)}{A(\theta_1)} = \frac{1}{F}\left[\frac{(n - \cos\theta_1)^3}{(n-1)^2(n\cos\theta_1 - 1)}\right]^{1/2} \tag{22}$$

An inspection of these equations shows that in Eq. (21) the amplitude ratio decreases with θ_1. That is, after leaving the lens the field is concentrated near its axis. The amplitude, in fact, drops to zero at the angle $\theta_{1\,max}$, given by Eq. (16). Therefore, this lens enhances the field taper of the source and is a good candidate for low sidelobe applications, but its aperture efficiency will be low. In contrast, the amplitude ratio in Eq. (22) increases with θ_1. That is, this lens corrects the amplitude taper of the source and enhances the aperture efficiency but, in the process, raises the sidelobe levels. Thus, it may be used in applications where the aperture efficiency is more critical than the sidelobe levels.

For most common dielectrics the refractive index is $n = 1.6$, that is, $\epsilon_r \cong 2.55$. For these materials the limit of the aperture angle is $\theta_{1\,max} = 51.3°$. Within this limit the amplitude ratios of Eqs. (21) and (22), normalized to axial values are shown in Table 1. The amplitude tapering of hyperbolic lenses is clearly evident. At 35° lens adds another 10 dB to the aperture field taper, and beyond 40° the lens is practically useless. For large-angle lens applications, higher dielectric constant materials must be used. Table 1 also shows the amplitude enhancement of elliptic lens. A 35° lens improves the aperture field uniformity by as much as 6.3 dB. It increases rapidly thereafter and becomes about 10 dB and 20 dB improvements for lens angles of 45° and 50°, respectively. These amplitude enhancements, however, must be accepted as theoretical limits, since at these wide angles the lens surface reflectivity will reduce the practically attainable levels. Surface matching layers must be used to minimize the reflections.

General Lens Design

In the general lens of Fig. 2, both surfaces are profiled and participate in collimating the beam. Thus, a more versatile lens can be obtained. However, Eqs. (1) to (6) showed that there are at least four unknown coordinates (x_1, y_1, x_2, y_2) to be determined. However, the optical relationships provided only three equations, which are not sufficient to uniquely determine the coordinates of both surfaces S_1 and S_2. Another relationship must be generated, which may be imposed on the amplitude distribution $A(\rho)$, to control the directivity or sidelobes. Alternatively, one may impose conditions on the aperture phase errors. An important case is the reduction of phase errors due to the source lateral defocusing. This will allow beam scanning without excessive degradation in efficiency and sidelobe levels. In most cases, however, the problem is too complex for an analytic solution and a numerical approach must be used.

ABERRATIONS

The term *aberration,* which originated in optics, refers to the imperfection of lens in reproduction of the original image. In antenna theory, the performance is measured in terms of the aperture amplitude and phase distributions. The phase distribution, however, is the most critical parameter and influences the far field significantly. It is therefore used in evaluating

Table 1. Amplitude Distributions for the Hyperbolic and Elliptic Lenses of Figs. 3 and 5

Amplitude Ratio, $\dfrac{A(\rho)}{A(\theta_1)}$		Ray Angle, θ_1 (deg)							
		0	10	20	30	35	40	45	50
Hyperbolic lens equation	Relative value	1.0	0.928	0.733	0.466	0.328	0.196	0.084	0.008
[Eq. (21)]	dB	0.0	−0.65	−2.70	−6.64	−9.70	−14.17	−21.5	−41.75
Elliptic lens equation	Relative value	1.0	1.060	1.26	1.69	2.06	2.67	3.17	9.25
[Eq. (22)]	dB	0.0	0.51	2.01	4.55	6.29	8.54	10.03	19.33

$n = 1.6$
$\epsilon_r = 2.55$
$\theta_{1\,\mathrm{max}} = 51.3°$

the performance of aperture antennas such as lenses and reflectors. With a perfect lens and a point source at its focus, the phase error should not exist. However, there are fabrication tolerances, and misalignments can occur that will contribute to aberrations. Even without such imperfections, lens antennas can suffer from aberrations. Practical lens feeds are horn antennas and small arrays. Both have finite sizes and deviate from the point source (2). This means that part of the feed aperture falls outside the focal point, and rays emanating from them do not satisfy the optical relationships. Thus, on the lens aperture the phase distribution is not uniform. Similar situations also occur when the feed is moved off axis laterally to scan the beam. Again, aperture phase error occurs due to the path length differences. A somewhat different situation arises when the feed is moved axially, front or back. In this case the phase error is symmetric, because all the rays leaving the source with equal angles travel equal distances and arrive at the aperture at an equal radial distance from the axis—that is, on a circular ring. However, the length of the ray increases, or decreases, with radial distance on the aperture. The phase error is, therefore, quadratic on the aperture and reduces the aperture efficiency, while raising the sidelobes.

The general aberration (i.e., the lens aperture phase error) can depend implicitly on both feed and lens coordinates and can be difficult to comprehend. However, like all other phase-error-related problems, it can also be represented as the path length difference with a reference ray. For rotationally symmetric rays, the natural reference is the axial ray. The path length difference can then be obtained by a Taylor-type expansion of the general ray length in terms of the axial one. For small aberrations the first few terms in the expansion will be sufficient to describe the length accurately. In terms of the aperture polar coordinates ρ and ϕ the expansion becomes

$$L(\rho,\,\phi) = L_{\mathrm{axial}} + \alpha\rho\cos\phi + \beta\rho^2[1 + \cos^2\phi] + \gamma\rho^3\cos\phi + \cdots \tag{23}$$

where α, β, and γ are constants indicating the magnitude of each phase error. The leading term is linear in ρ and ϕ, then becomes quadratic, cubic, and so on, and the magnitude of each depends on the nature of imperfection causing the phase error. The even terms are caused either by an axial defocusing or by an axially symmetric error. The odd terms can be due to a lateral displacement of the feed or can be due to asymmetric errors.

The effects of each error can be investigated by its introduction in the aperture field and determining the far field using a Fourier transformation or diffraction integral. For one-dimensional errors (i.e., $\rho = x$ and $\phi = o$) the effect can be understood easily and has been investigated by Silver (1). The first term is linear, and in a Fourier integral it shifts the transform variable. It thus causes a tilt of the beam, but the gain remains the same. Using Silver's notation, if $f(x)$ is the aperture distribution and $g(u)$ is the far field (i.e., its Fourier transform with a linear phase error), one finds with no phase error

$$g_0(u) = \frac{a}{2}\int_{-1}^{1} f(x)\,\exp[jux]\,dx \tag{24}$$

and with phase error

$$g(u) = \frac{a}{2}\int_{-1}^{1} f(x)\exp[j(ux - \alpha x)]\,dx = g_0(u - \alpha) \tag{25}$$

where $u = (\pi a/\lambda)\sin\theta$ and a is the aperture length. Equation (25) shows that the beam peak is moved from the $\theta = 0$ direction to θ_0, calculated by

$$u - \alpha = 0$$

or

$$\theta_0 = \sin^{-1}\left(\frac{\alpha\lambda}{\pi a}\right) \tag{26}$$

A quadratic phase error is symmetric on the aperture and does not tilt the beam, but reduces its gain. For small values of β, it can be calculated analytically (1) and is given by

$$\begin{aligned}
g(u) &= \frac{a}{2}\int_{-1}^{1} f(x)\,\exp[j(ux - \beta x^2)]\,dx \\
&\cong \frac{a}{2}[g_0(u) + j\beta g_0''(u)]
\end{aligned} \tag{27}$$

where $g_0''(u)$ is the second derivative of $g_0(u)$. Due to this phase error the gain decreases progressively with increasing β, and eventually the beam bifurcates and maxima appear on either
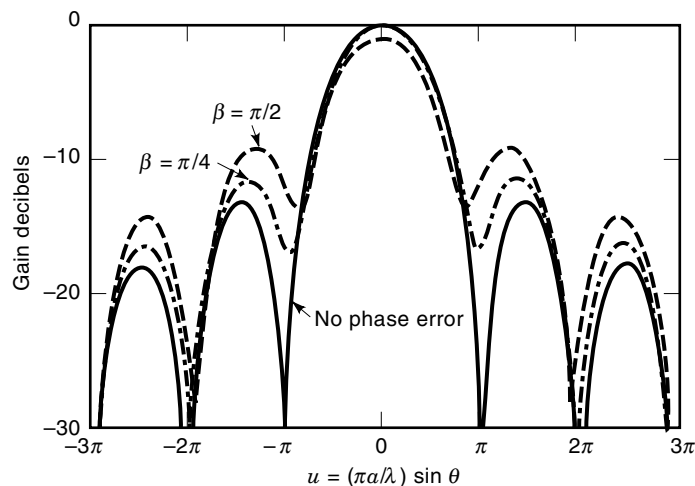
Figure 6. Effect of quadratic phase error on the far-field pattern.

side of the axis. It also raises the sidelobe levels. Figure 6 shows typical pattern degradation due to this error.

The next important phase error is the cubic one, which has odd power dependence on the aperture coordinate. This error not only tilts the beam, but also reduces the gain and asymmetrically affects the sidelobes, raising them on one side while reducing them on the opposite side. Its effect is therefore a combination of that of the linear and quadratic phase errors. For small errors its far field is given by (1)

$$g(u) = \frac{a}{2} \int_{-1}^{1} f(x) \, \exp[j(ux - \delta x^3)] \, dx$$
$$\cong \frac{a}{2} \, [g_0(u) + \delta g_0'''(u)]$$

(28)

where $g_0'''(u)$ is the third derivative of $g_0(u)$. For a few small phase errors the far fields of this phase error are shown in Fig. 7. They show clearly the beam tilt, the gain loss, and the rising of the sidelobes toward the beam tilt. They are known as coma lobes, after the corresponding aberration in optics. Also, because this phase error causes more severe pattern
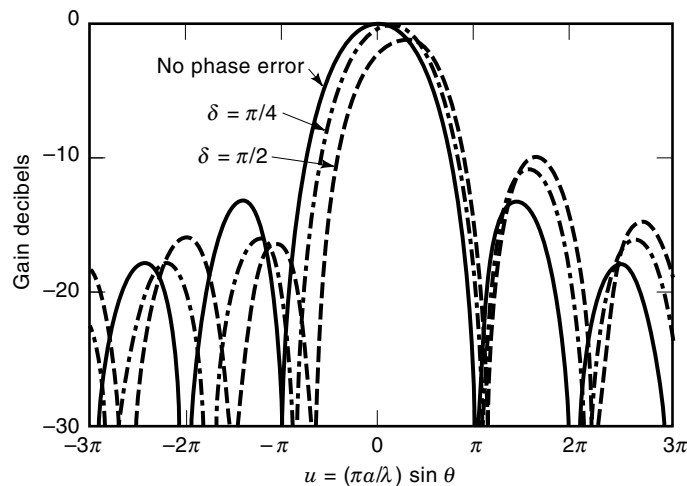

Figure 7. Effect of cubic phase error on the far-field pattern.

degradation than others, it is desirable to eliminate it, especially that it manifests mostly in beam scanning. Feed lateral displacements to scan the beam can readily cause coma lobes. Fortunately, a number of lens surface modifications have been found to reduce the effects of this error (3).

ZONED LENSES

So far, the equations used for lens design equalized the ray path lengths. The frequency of operation, or its wavelength, did not enter into the equations. Thus, in principle, these lenses should function at all frequencies. However, the directivity of a lens depends on its aperture size D, and these lenses are often used for high gain applications. This results in large lens sizes in wavelength; and at microwave frequencies, in large physical sizes, both the aperture diameter D and thickness T. It can, therefore, become excessively heavy and difficult to use. However, the thickness of the lens can be several wavelengths, and thus it can be reduced along the ray path in multiple wavelengths without altering the relative phase change. The process starts at the edge where the thickness is zero. Moving down toward the axis, the thickness increases progressively until it becomes one wavelength. This thickness can be made zero without altering the phase. The process can be continued K times until one arrives at the lens axis. In practice, one must maintain a small thickness t_m to provide adequate mechanical strength, the value of which will depend on the lens size, the material strength, and application type.

With zoned lenses, and neglecting t_m because the thickness does not exceed one electrical wavelength, its thickness is limited to $\lambda/(n - 1)$. Including the minimum thickness t_m, the total thickness is limited to $t_m + l/(n - 1)$ regardless of the number of zones. The path lengths in wavelength, however, are not equal. With K zones, the ray path at the edge will be longer by a length equal to $(K - 1)\lambda$. This causes the frequency dependence of lens operation, limiting its bandwidths. Enforcing the commonly used Silver's criterion for this aperture phase error (1) (i.e., less than 0.125λ), the useful bandwidth of a lens with K zones can be calculated from (1)

$$\text{Bandwidth} \cong \frac{25}{K - 1}\%$$

(29)

Equation (29) is valid for small variations of λ and uniform aperture distributions. For taper distributions the effects of phase errors is smaller and the actual bandwidth can exceed that of Eq. (29).

Zoning the lens can cause one additional, severe problem due to shadowing. Two adjacent rays from the focus can travel through two separate zones, resulting in a dark ring zone on the aperture. This occurs in the transmit mode, and it causes the loss of directivity and increased sidelobe levels. In the receive mode, the energy falling on the shadow zones never reaches the lens focus and diffracts into the space, again causing reduction of gain along with increased noise temperature. Figure 8 shows the geometry of a three-zone lens and shadowing due to R_1 and R_2 rays.

Zoning without shadowing is also possible, but should be done on the nonrefracting surface of the lens. In a hyperbolic lens, this should be done on the planar back surface. Shadow-
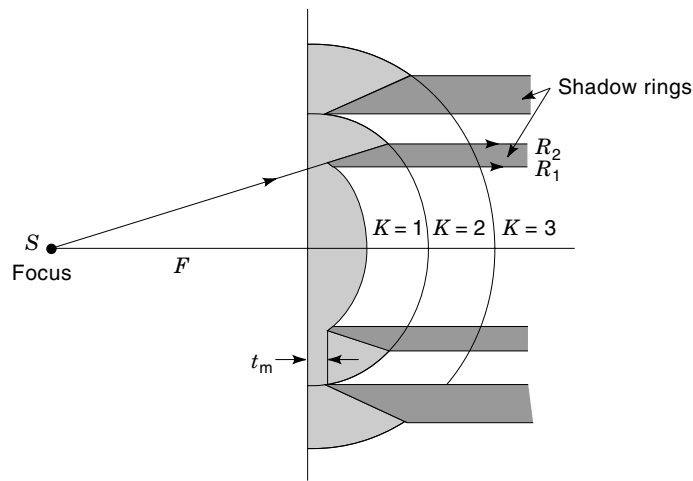
Figure 8. Geometry of a zoned lens with shadowing effects.

ing will be eliminated, but phase errors still occur at the transition lines due to diffraction effects.

REFLECTION FROM LENS SURFACE

Because the wave impedance in air and the dielectric medium of lens are different, reflections occur for all the rays. The reflection coefficient depends both on the wave polarization and the angle of incidence—that is, the angle of ray with the local normal on the lens surface. Neither can be avoided. With a linearly polarized wave, the relative polarization, with respect to the plane of incidence, changes from perpendicular to parallel as the ray direction rotates on the lens surface. However, their reflection coefficient behaves differently. For perpendicular polarization, it increases progressively with the incidence angle. For parallel polarization, it decreases initially; and after vanishing at the Brewster angle, it increases rapidly. Consequently, incidence angles must be kept small, less than 30°, to minimize the polarization effects on the lens aperture distribution.

The surface reflection effects can be reduced when warranted, but this requires utilizing an impedance matching layer between the lens and free space. At normal and small angles of incidence, the refractive index of the matching layer can be found using a quarter-wavelength transformer rule. It is the geometric means of the refractive index of the lens dielectric and that of air. In practice, a different dielectric material may be used as the matching layer, or it may be synthesized by preferentially removing a fraction of the dielectric material from the lens surface, such as drilling $\lambda/4$ holes or cutting grooves (4). However, care must be taken to determine their polarization effects.

The surface reflections also influence the impedance mismatch at its feed. The problem is most severe in cases where the lens surface is coincident with one of the equiphase surfaces—that is, the wave front. Then, the entire reflected wave travels back to the feed, the degree of which depends on the lens refractive index. Since at normal incidence the reflection coefficient is $|R| = (n-1)/(n+1)$, the reflected power is unacceptably large for all common dielectrics, and a matching surface should be used. In the event a matching layer cannot be used, the reflection effects on the feed can be minimized by lateral defocusing of the feed, or retuning of the feed over a narrow bandwidth.

LENSES WITH $n < 1$

Lens equations (1) to (6) were developed without specifying the value of the refractive index, and therefore they are valid for $n < 1$ cases as well. However, the lens surface becomes inverted. For instance, the hyperbolic lens equation [Eq. (13)] for $n < 1$ modifies to

$$r_1 = \frac{(1-n)F}{1 - n\cos\theta_1} \tag{30}$$

and the lens surface becomes elliptical, concave toward the focus, similar to Fig. 1(b). On the inner region a minimum thickness t is required to provide mechanical strength. Zoning is also possible and will cause shadowing when incorporated on the active refracting surface. The bandwidth limitations due to n remains the same as the dielectric lenses with $n > 1$. However, the lens media for $n < 1$ such as metal plates and waveguides are usually frequency-sensitive and exhibit narrower bandwidths.

CONSTRAINED LENSES

The function of a lens is to modify the phase front of an incident wave, say from spherical to planar. In practice, this may be accomplished by means other than the dielectric lenses. In the most general case, the lens surfaces consist of a plurality of receiving and radiating elements, interconnected by processing elements. The received signals of one surface are modified in amplitude and phase and are reradiated from the elements of the next surface. In passive designs, the interconnection is due to transmission lines, such as parallel plates, waveguides, and even coaxial lines. The design process is similar to that of the dielectric lenses and is governed by the path-length equation. Snell's law, however, is not satisfied at all surfaces, and the problem of surface reflection and transmission must be solved through the use of the wave equation. Nevertheless, lenses can be designed with surfaces similar to that of dielectric lenses, but with inverted curvature (3).

The simplest case uses parallel plates, with spacing a, between one and one-half wavelength. When the electric field is parallel to the plates, a non-TEM waveguide mode is excited and has a wavelength λp given in terms of the free space wavelength λ by

$$\lambda p = \frac{\lambda}{\left[1 - \left(\frac{\lambda}{2a}\right)^2\right]^{1/2}} \tag{31}$$

which can be used to define an equivalent refractive index as

$$n = \frac{\lambda}{\lambda p} = \left[1 - \left(\frac{\lambda}{2a}\right)^2\right] < 1 \tag{32}$$

In cylindrical lenses, when the plates and electric field are normal to the cylinder axis, Snell's law of refraction governs

the transition between the lens and outside media. But, when they are parallel to the cylinder axis, the incident rays are constrained to pass between the plates and Snell's law is not satisfied (1).

An example of the rotationally symmetric constrained lens is the planar–elliptic surface lens of Eq. (30). It is usually zoned to reduce its size and weight (4). Other useful transmission media are the rectangular and square waveguides, operating in TE_{10} or TE_{01} modes. The waveguide dimensions must be such that only these modes can propagate and higher-order modes are suppressed. The square waveguide can be used for circularly polarized applications; otherwise, it must be avoided to reduce cross-polarization.

INHOMOGENEOUS LENSES

In the lenses so far studied, the refractive index n was constant and the shape was profiled to satisfy the ray path condition. On the other hand, if the lens shape is kept fixed, then another parameter, such as the refractive index, must be allowed to change to help in collimating the beam. This is achieved in a family of lenses, with the most important ones being spherical in shape, such as Luneberg lens, Maxell's fisheye, and Eaton lenses. Their spherical shape provides a perfect three-dimensional symmetry, useful in applications, such as wide-angle scanning. They also have only a radial inhomogeneity, making them both physically and electrically symmetric.

Luneberg Lenses

The Luneberg lens refers to a family of lenses with two axial foci. They can be both outside the lens or one inside and the other outside. The most useful case, however, is the lens with one focus on its surface, while the second one is at infinity. That is, an axial point on the lens surface is focused to an axial point at infinity, on the opposite side of the lens. The refractive index of this lens is given by

$$n(r) = \left[2 - \left(\frac{r}{a} \right)^2 \right]^{1/2} \qquad (33)$$

where a is the lens radius and r is the radial distance of a point inside the lens. At the origin, the refractive index is $n(o) = 2$, and on its surface it becomes unity. Both are practi-
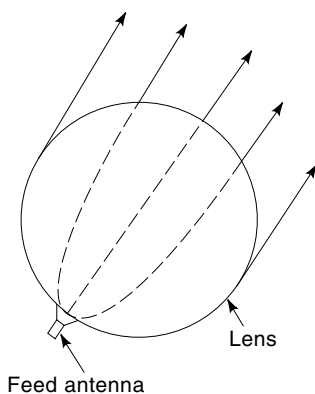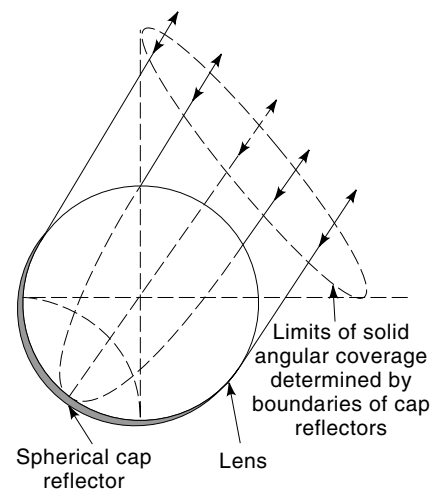

Figure 10. Passive Luneberg lens reflector.

cally significant. The refractive index values and variations are in reasonable range, and the lens can be synthesized. Second, the unity of its refractive index on the surface eliminates the impedance mismatch and, consequently, the surface reflections. The geometry and ray paths of this lens are shown in Fig. 9, with a feed horn on its surface. Scanning the feed on its surface scans the radiated beam, without alteration. The scan limit is set only by the mechanical limitation of the feed horn motion. With a spherical conducting cap on its surface the lens also acts as perfect reflector—that is, a backscatter (Fig. 10). The main difficulty with this lens is its fabrication problems. Multilayer shells are normally used to synthesize the refractive index inhomogeneity. Figure 11 shows one case where 10 layers are used to construct an 18 in. diameter lens. While the approximation to continuously variable refractive index is reasonable, the wave scattering at the layer transitions reduces the lens efficiency.

With the above refractive index, the Luneberg lens performance is ideal at the geometrical optics limits—that is, when
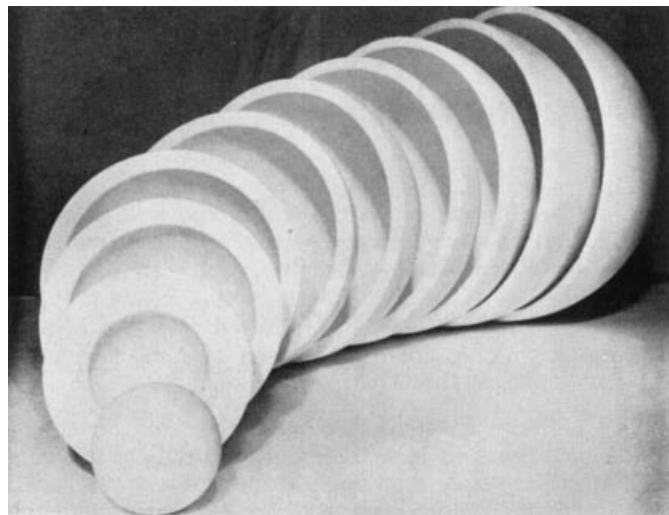

Figure 9. Typical ray paths in a Luneberg lens.

Figure 11. Multilayer spherical shell construction of a Luneberg lens.
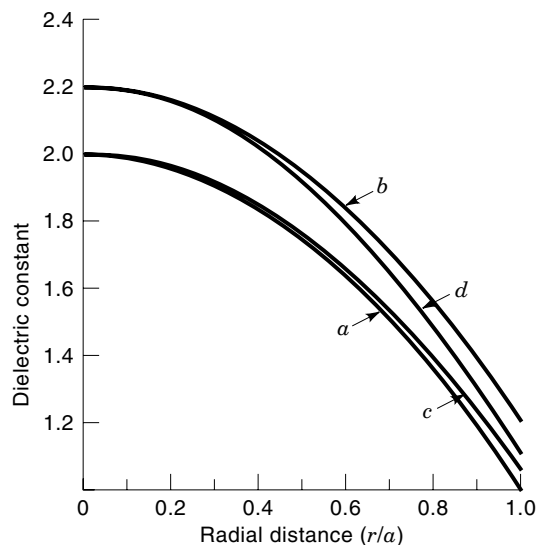
Figure 12. Refractive index of modified Luneberg lenses.

Figure 13. Phase across aperture of a constant n spherical lens.

the lens diameter in wavelength is large. At microwave frequencies, the wavelength is large and the lens diameter in wavelength may not be large. Its performance (i.e., directivity) and sidelobe levels deteriorate rapidly. In such cases, the refractive index profile can be modified to improve its performance. This can be done by determining the excitation efficiencies of various spherical modes and calculating its far field and directivity (5). The new dielectric permittivity profile is defined as

$$\epsilon_r = n^2 = 2B - A^2 \left(\frac{r}{a}\right)^2 \qquad (34)$$

where the constant parameters A and B are determined to maximize the gain. Three different cases are identified and investigated. Their refractive index profiles are shown in Fig. 12. Cases (b) ($A = 1$, $B = 1.1$) and (c) give larger refractive indexes and are expected to perform better at lower frequencies. This is investigated using the spherical harmonies, and the results for the directivity, sidelobe levels, and beamwidths are shown in Table 2.

Constant *n* Spherical Lens

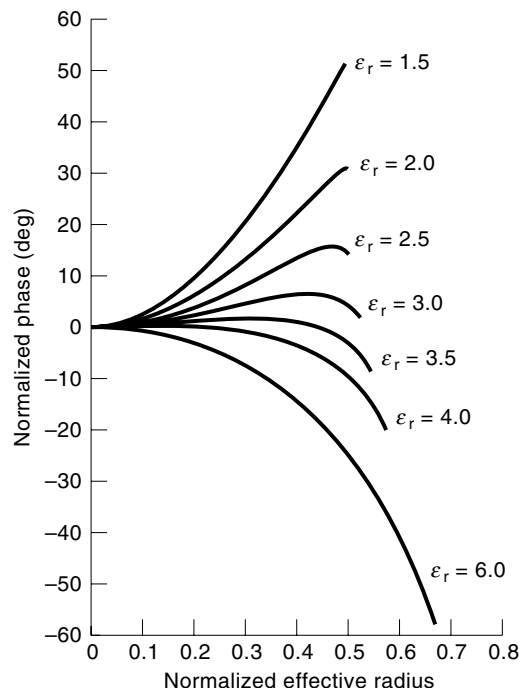The difficulty with fabrication of the inhomogeneous lenses encouraged investigators to search for quasi-ideal spherical lenses with constant refractive index. An interesting case is a lens with $\epsilon_r \cong 3$, studied earlier by Bekefi and Farnell (6) and recently by Mason (7). With a Huygen source feed at its surface, the computed phase distribution across its aperture, for different relative permittivities are shown in Fig. 13. For $\epsilon_r \cong 3$, the phase error is below 10°, across about 60% of the aperture. It remains within acceptable range for gain calculating over at least 70% of the aperture, resulting in excellent gain performance over a wide range of frequencies. The only drawback seems to be the excitation of internal modes at their resonance. Their effect reduces with the loss tangent of the dielectric material.

DIELECTRIC LOADED HORNS

Horn antennas are among the most useful and versatile antennas. They have a relatively simple shape and are easy to fabricate and use. They are used as test antennas, as feeds for reflector and lens antennas, or independently as communi-

Table 2. Performance Parameters of Modified Luneberg Lens

| | | Luneberg Lenses | | | Modified Luneberg Lenses | | | | | |
| | | A = B = 1 | | | A = 1 | | | A² = B | | |
Diameter in λ	B Value	Gain (dB)	Beam Width (degrees)	First Side-Lobe Level (dB)	Gain (dB)	Beam Width (degrees)	First Side-Lobe Level (dB)	Gain (dB)	Beam Width (degrees)	First Side-Lobe Level (dB)
2	1.4	14.79	30.2	−14.41	17.56	23.5	−17.15	16.85	24.0	14.79
4	1.16	20.761	15.1	−16.05	22.70	13.0	−16.9	22.0	13.25	−16.1
6	1.1	24.34	9.8	−16.9	25.75	9.0	16.97	25.17	9.1	−16.4
8	1.075	26.90	7.3	−17.1	27.98	6.7	−17.01	27.56	7.0	−16.6
10	1.04	28.78	5.8	−16.35	29.35	5.5	−15.97	29.26	5.6	−16.81

cation antennas. Because of their diverse applications, their electrical specifications vary considerably. As test antennas, they are used as gain standards and required to have good polarization isolation in the principal E and H planes. Rectangular horns are commonly used for this application to simplify the polarization definition and gain calculation. As a feed for reflector and lens antennas, the requirements are significantly different. While having a finite aperture size, they must behave as a point source, have small side and back lobes to minimize power spillovers, and have negligible cross-polarization in the entire radiation zone. To achieve such stringent requirements, their design must be precise and an accurate solution must be known to access their performance. This is more so with circular horns, which, consequently, have found more widespread applications as feeds than rectangular ones. The electromagnetic analysis, however, has shown that conventional smooth wall horns cannot provide radiation patterns with acceptable polarization purity and low spillover. Corrugated horns are developed for these applications, but are costly and narrowband. Dielectric loading of the horn has been shown to improve the performance as well, and in certain applications it may be used to replace corrugated ones.

In applications where horn antennas are used as independent communication antennas, the gain and aperture efficiency may be the fundamental parameters to optimize. However, to obtain high gains, the horn aperture size must increase, which also increases the aperture phase errors. The phase errors can be kept low by using small cone angles, but this increases the horn size. Thus a convenient solution involves the use of a lens at the horn aperture to reduce or eliminate the phase errors, by collimating the beam. Consequently, compact high gain horns can be designed with controlled aperture phase and amplitude distributions, to improve the aperture efficiency and horn gain. Alternatively, lenses can be used to suitably modify the aperture distribution in both amplitude and phase to shape the radiation patterns.

In this section, initially the dielectric loaded and lens corrected horns will be discussed. Then the use of dielectric in small antennas such as waveguides, microstrip antennas, and dipoles to improve their operation in specific applications will be considered.

Dielectric Loading

Historically, dielectric-cone loading inside smooth wall conical horns was used by Clarricoats et al. (8) and Lier (9) to simulate the effect of corrugations. Corrugated horns, with quarter-wavelength corrugation depths, can support the hybrid HE_{11} mode. This mode radiates with low cross-polarization and can be designed to have negligible sidelobes. Introduction of the cone dielectric, with an air gap as shown in Fig. 14 inside a smooth wall horn, was shown also to support hybrid modes and improve the performance. Clarricoats et al. (8) used low-dielectric-constant materials, such as foams with a relative permittivity of 1.13. But, in Lier's work (9), solid-dielectric cones with a relative permittivity of 2.5 were used, again showing good performance. Both investigators also analyzed these dielectric loaded horns using modal expansions, and they studied the effects on the air gap, horn permittivity, aperture diameter, flare angle, and the throat region. It was found that the air gap size is strongly dependent on the aper-
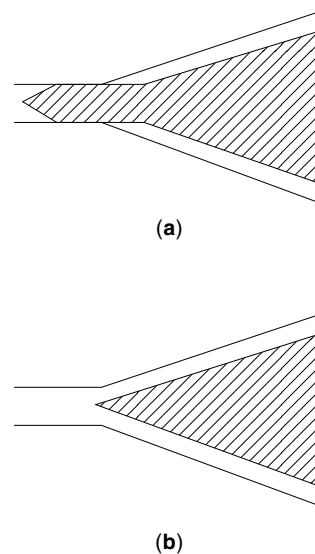
(a)

(b)

Figure 14. Geometry of a dielectric loaded horn.

ture diameter, and both are dependent on the dielectric permittivity. The air gap size generally increases with the horn diameter, and for a given diameter there is a minimum relative permittivity of dielectric to support the hybrid mode to minimize the cross-polarization. Both flare angle and the throat region have similar influences. Large flare angles and an asymmetric throat region design excite higher-order modes and thus increase cross-polarization.

A variation of the conical dielectric loaded horn is shown in Fig. 15. Its wall is profiled. A large flare angle near its throat reduces its axial length and results in a compact horn. Then, its small flare angle near the aperture improves its cross-polarization. The profile is described by the following equation:

$$r(z) = r_{\text{th}} + 3\Delta r \left(1 - \frac{2z}{3L}\right)\left(\frac{z}{L}\right)^2$$

$$\Delta r = r_{\text{ap}} - r_{\text{th}}$$

(35)

where r_{ap} and r_{th} are the horn radii at its aperture and throat. A profile horn of this type was designed and optimized. Its
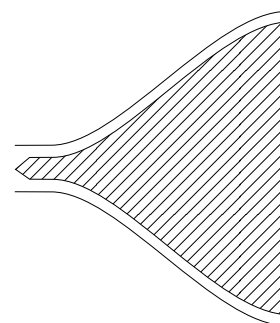
Figure 15. Geometry of a dielectric loaded profile horn.

Table 3. Performance of Dielectric Loaded Linear and Profiled Horns

Parameter	Linear Horn	Profiled Horn
3 dB beam width (degrees)	14.8	13.7
10 dB beam width (degrees)	26.9	24.8
Directivity (dB)	22.1	22.5
Efficiency (percent)	61.8	68.1
Peak cross-polar (dB)	−32.2	−36.0
VSWR	1.04	1.03

R_{th} = 1.14 cm
r_{up} 27.7 cm
L = 30.9 cm
ϵ_r = 1.13
Air gap = 1.2 cm

performance is compared with the linear horn in Table 3. Its cross-polarization is improved by 4 dB. The effect of length reduction on the performance of the above profile horn is also shown in Table 4. It shows that the performance remains steady and comparable to a linear horn, for length reductions by as much as 22%.

Lens Corrected Horns

In high-gain horns, the aperture diameter in wavelength is large, and the horn length can be excessive, unless its flare angle is made large. However, the combination of large aperture size and large flare angle can cause severe aperture phase error. This problem can be remedied by using a lens at the horn aperture. Figure 16 shows three possible options. These simple lenses and others including zoned lenses may be used, and they would correct the horn aperture phase distributions. But each lens will have different influences on the aperture amplitude distribution. The case of the first two lenses were investigated earlier, and Table 1 showed their effect on the amplitude distribution. Type a increases the amplitude taper according to Eq. (21) and will reduce both sidelobes and the aperture efficiency. Type b will compensate for the amplitude taper, and according to Eq. (22) the lens permittivity can be used to control the aperture distribution and, hence, the horn efficiency and the pattern sidelobes. For type c, an analytic expression is not available and a numerical procedure must be used. However, as was indicated earlier in this lens, both surfaces help collimating the beam. But its second surface is similar to type b lens, and its influence on the aperture distirbution will be similar as well. With a hybrid mode horn, corrugated or dielectric loaded, the resulting aperture distributions for different lens relative permittivity

Table 4. Performance of Profile Horn with Length Reduction

Length (cm)	Peak Cross-Polar (dB)	3 dB Beamwidth (deg)	Efficiency %
30.9	−36.0	13.7	68.1
27.5	−36.8	13.8	64.4
24.0	−31.6	14.0	57.1
15.0	−27.6	16.1	32.0
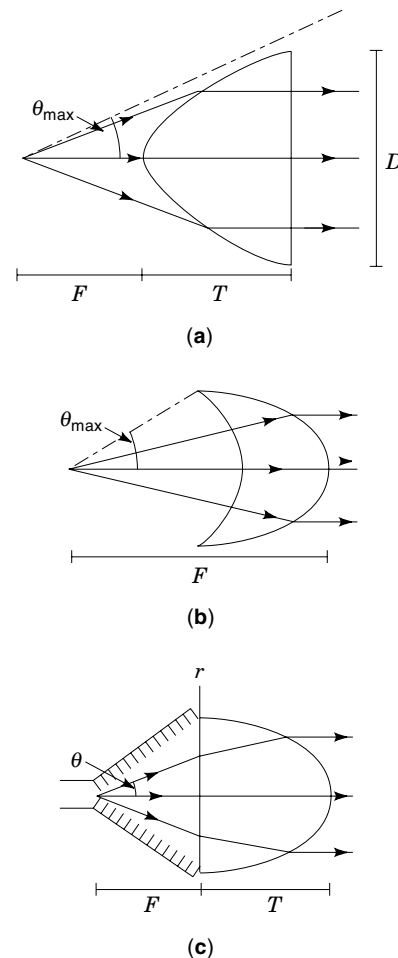
Figure 16. Lens types for loading horn aperture.

are shown in Fig. 17. It shows that for ϵ_r around 1.22 the aperture amplitude distribution is nearly uniform.

DIELECTRIC LOADED WAVEGUIDES

Waveguides have small aperture size and are not as efficient radiators as horns. Part of the energy leaks out and induces current on the outside wall, which radiates side and backward, causing large back lobes. The wave impedances of waveguide modes are also different from the free-space intrinsic impedance and strong reflections can occur on the aperture, causing poor input impedance match. These problems can be partly overcome by flaring the waveguide at its aperture. However, a similar and even better performance can be obtained by loading the waveguide by a short section of a dielectric. The constant, size, and shape of a dielectric provide several parameters that can be used to shape the radiation patterns and tailor them to desired specifications. Table 5 shows the results for three different end loadings, along with the type of performance variations one could achieve (2). Two other examples are shown in Figs. 18 and 19, with combinations of dielectric and cavity loadings (2). In Fig. 18, the end geometry is optimized for nearly perfect pattern symmetry, with negligible cross-polarization. Figure 20 shows its copolar and cross-polar radiation patterns. In Fig. 19, again the com-
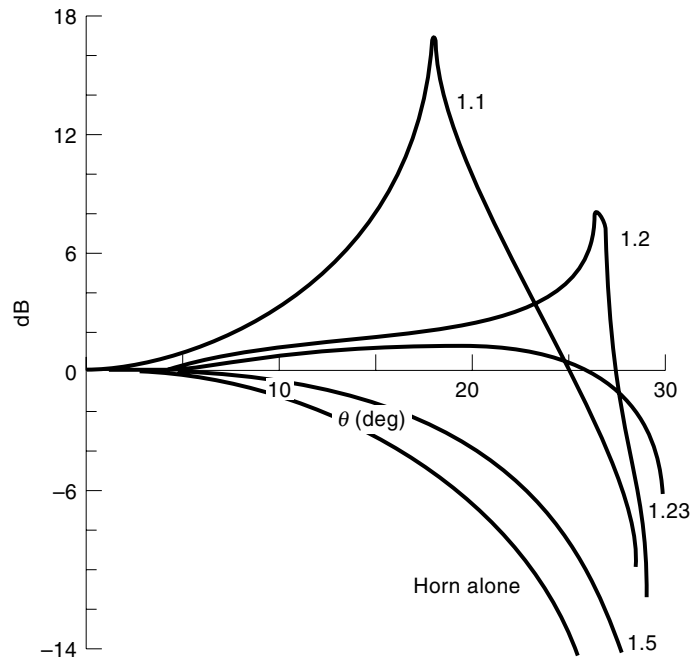
Figure 17. Aperture amplitude distribution for a lens corrected horn, 30° semiflare angle hybrid mode horn, type *c* lens.

bination was optimized for a heavily shaped radiation pattern with again negligible cross-polarization in the forward direction. It is an ideal feed for deep parabolic reflectors with small $f/D = 0.25$. It provides high aperture efficiency of 81% due to its front pattern null, very low cross-polarization, and extremely low noise temperatures due to small f/D, the focal-length-to-diameter ratio.

MICROSTRIP AND DIELECTRIC RESONATORS

Microstrip antennas are discussed in a separate article, and they usually consist of a conducting patch separated from
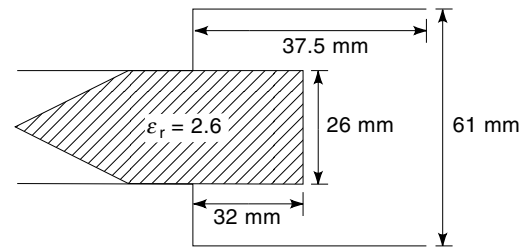
Figure 18. Geometry of a dielectric and cavity loaded waveguide feed.

a ground plane by a dielectric substrate. They are low profile and increasingly popular antennas for practically any type of applications. Their radiation patterns, however, are asymmetric with unequal E- and H-plane patterns. But, with careful optimization, the pattern symmetry can be achieved to minimize cross-polarization. Figure 21 shows a case of stacked patches with a side choke for equalizing the principal plane pattern, low back radiation, and cross-polarization. Similar performance can also be obtained using a dielectric resonator in lieu of a microstrip patch. The dimensions of the dielectric resonator are related to the wavelength by

$$d = \frac{1.841\lambda}{4n\pi}\left[16 + \left(\frac{\pi d}{1.841h}\right)^2\right]^{1/2} \qquad (36)$$

The excited mode is the TM_{110} mode, and it gives radiation similar to that of a microstrip patch. In Fig. 22, the resonator and the cavity are optimized for symmetric pattern in the principal planes to reduce the cross-polarization. They are shown in Fig. 23, with excellent symmetry. Both the microstrip and resonator antennas can be used as efficient reflectors and lens feeds with high aperture efficiency and low cross-polarization.

Table 5. Performance of Dielectric Loaded Waveguide with Shaped Dielectrics

Geometry	Peak Cross-Polarization $0 \le \theta \le 90°$ (dB)	Gain (dB)	Half-Beamwidths			
			3 dB		10 dB	
			E Plane	H Plane	E Plane	H Plane
a	−33.95	8.28	36.82	36.18	71.47	72.51
b	−24.74	8.11	37.21	38.32	73.42	71.35
c	−24.43	13.47	19.43	20.25	33.13	35.17

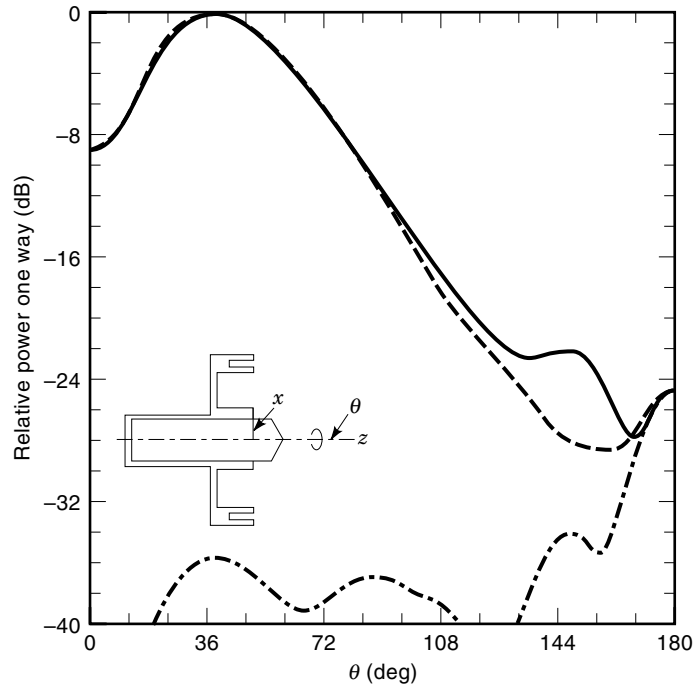$D = 0.6\lambda$, $\epsilon_r = 2.5$

Figure 19. Geometry and radiation pattern of a shaped dielectric and cavity loaded waveguide feed.

INSULATED ANTENNAS

Practically all antennas have conducting parts, but in certain families of antennas, especially small resonant ones, the conduction current radiates directly. Typical examples are the wire antennas and microstrip antennas that are often half-wavelength resonators. In wire antennas, the current is excited by the applied voltage directly on the wire, which radiates in the surrounding space. In microstrip antennas, the currents are both on the patch and on its ground plane, which are separated by a dielectric substrate. Because of this, only the patch current is exposed to the surrounding medium. However, in either case, the physical constants of the medium is excessively lossy: It can short-circuit the antenna current and prevent its operation. In practice, this problem can occur in remote sensing and biological applications. In the former case, the antennas may be buried underground or may be submerged in sea and ocean waters, which have high electrical conductivities. In the latter case, the antennas are implanted into various type tissues in the body that can have excessively high conductivities. In such cases, to ensure the antenna operation, the conduction currents must be insulated from the surrounding conducting medium. A simple but effective method is to use a thin dielectric coating on the antenna conductor carrying the radiating currents. The coating will provide insulation between the conducting antenna and the medium, thereby eliminating the conduction current. The excitation energy will then transfer into the poynting vector, leaving the antenna.

The behavior of the insulated antennas in a medium of complex permittivity differs considerably from that in free space, and it should be analyzed carefully. For instance, consider a conventional dipole of length $2h$, as shown in Fig. 24. The wire is a good conductor and has a diameter
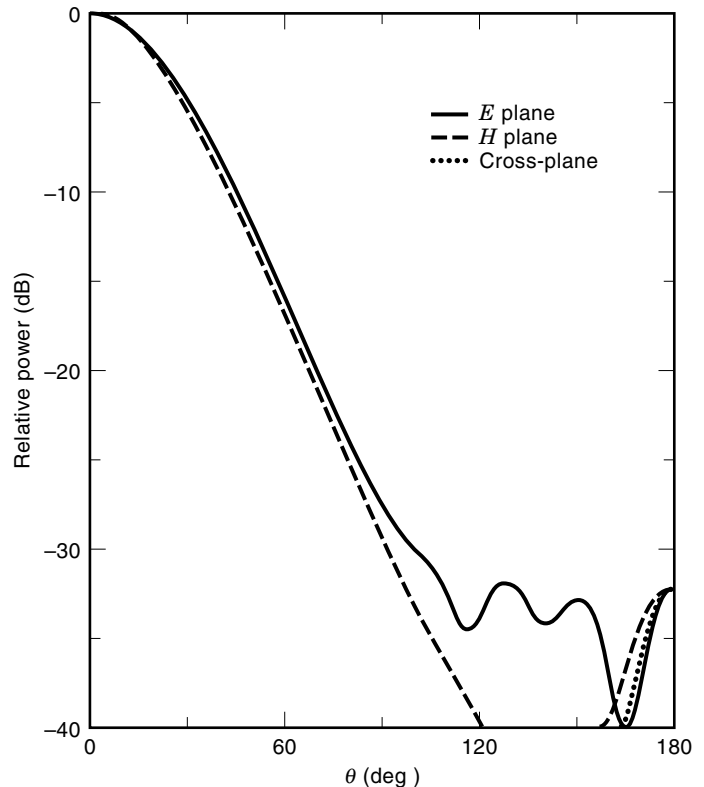

Figure 20. Radiation patterns of the waveguide feed of Fig. 18.

of $2a$, insulated by a cylindrical dielectric region of diameter $2b$ and propagation constant k_1, located in an infinite exterior region of k_2. With a thin-wire approximation, the dipole current can be represented by a sinusoidal distribution of the form (10). The time factor is assumed as $\exp(j\omega t)$:

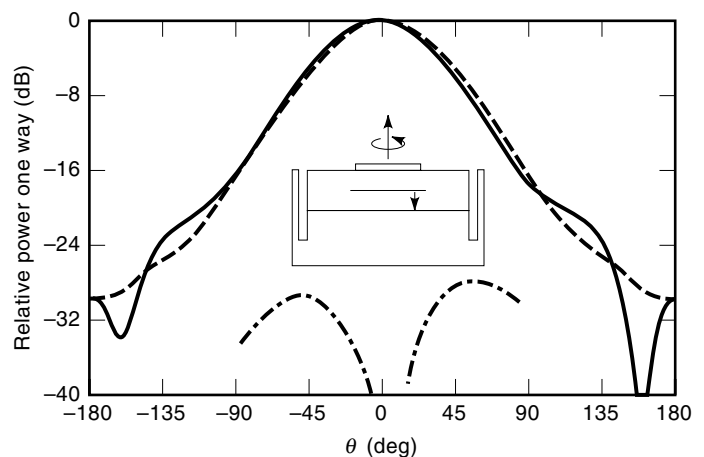$$I(z) = \frac{-jV \sin k_{\mathrm{L}}(h - |z|)}{2Z_{\mathrm{ca}} \cos k_{\mathrm{L}} h} \tag{37}$$

Figure 21. Geometry and radiation patterns of a stacked microstrip feed.
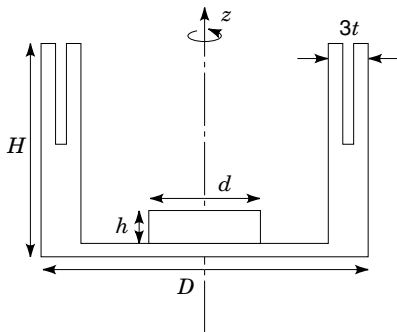
Figure 22. Geometry of a dielectric resonator antenna.

where

$$k_{\mathrm{L}} = k_1 \left[1 + \frac{H_0^{(2)}(k_2 b)}{k_2 b H_1^{(2)}(k_2 b) \ln \dfrac{b}{a}} \right]^{1/2} \tag{38}$$

$$Z_{\mathrm{ca}} = \frac{\zeta_1 k_{\mathrm{L}}}{2\pi k_1} \ln \left(\frac{b}{a} \right) \tag{39}$$

$$\zeta_1 = \frac{\omega \mu_0}{k_1} \tag{40}$$

$$k_1 = \omega [\mu_1 \epsilon_1]^{1/2} \tag{41}$$

And $H_0^{(2)}$ and $H_1^{(2)}$ are Hankel functions of zero and first order. Note that with a perfect insulation dielectric, k_1 is real; but k_2 is complex due to the presence of Hankel functions in Eq. (38). It reduces to k_1 when b, the radius of the insulation, becomes infinitely large. In view of Eq. (38) the dipole current distribution, input impedance, radiation resistance, and resonance frequency can depend strongly on the radius b, propagation constant k_1, and the propagation constant of the exterior region, k_2. The latter may not be fully known, or constant, during the application due to variations in moisture content,
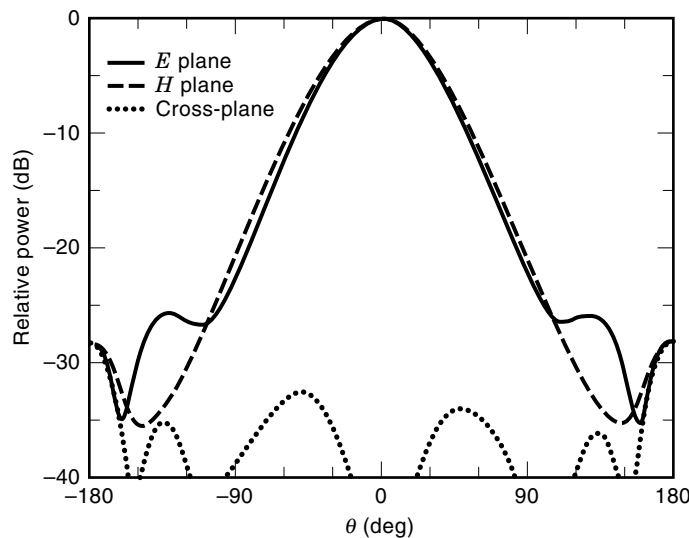

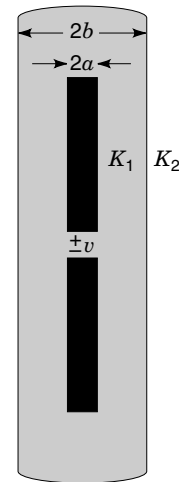**Figure 23.** Radiation patterns of the dielectric resonator antenna.

Figure 24. Geometry of an insulated dipole antenna.

and so on. Thus, the insulation parameters should be selected appropriately to minimize the dependence of k_1 and k_2.

MEDICAL AND BIOLOGICAL ANTENNAS

Another area that insulated antennas play an important role in is the biological and medical applications. They can be non-invasive (i.e., not penetrating the body) or invasive. In either case, the property of insulated antennas can be significantly different from those in free space. Thus, care must be taken in their design and analysis to ensure adequate power transfer to the right tissue. Noninvasive radiators are often dielectric loaded waveguides and horns, discussed in the previous section. The dielectric loading in this case is used to improve impedance matching and coupling to the body. Their design is not significantly different from other dielectric loaded waveguides, except that the end shaping must prevent hot spots and improve penetration.

Microstrip antennas and arrays are another type of radiators suitable for noninvasive applications. However, their resonance property and power coupling to the body can be sensitive to the extent and nature of contact to the skin. Dielectric coating over the radiating patch or slot can insulate the antenna and minimize the body's influence. This is due to the fact that in microstrip antennas the resonance depends on the effective dielectric constant, and not the actual substrate permittivity. With single-layer substrates of thickness h, this effective permittivity, for a conductor line width of W, is given by

$$\epsilon_{\mathrm{eff}} = \frac{\epsilon_{\mathrm{r}} + 1}{2} + \left(\frac{\epsilon_{\mathrm{r}} - 1}{2} \right) \left(1 + \frac{12h}{w} \right)^{-1/2} \tag{42}$$

However, it can change significantly by introducing a higher permittivity layer over the substrate. Consequently, in biological applications, where the tissue relative permittivity can be excessively high, due to the water content having $\epsilon_{\mathrm{r}} \cong 80$, the nature of the proximity or contact with body can alter ϵ_{eff} significantly (11). Because microstrip antennas are narrowband, or at best not wideband, the efficiency of their radiation and coupling to the body can be deteriorated. The effect can be
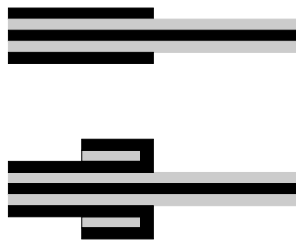
Figure 25. Implantable radiator types. (a) Needle radiator, (b) sleeve antenna.

reduced by introducing a superstrate layer over the microstrip antenna to control the relative permittivity variations.

Invasive-type radiators can produce more uniform and controllable heating patterns, but they require implantation in the tissue. The most convenient types are the insulated needle radiator, basically the end of the coaxial line. However, this type of antenna can generate strong currents on the outer coaxial conductor and cause tissue heating behind the antenna. An improvement can be obtained by introduction of a quarter-wavelength choke over the coaxial conductor to form a sleeve antenna. Their analysis and sensitivity study can be carried out similar to the insulated dipole antennas. Figure 25 shows the geometry of needle and sleeve antennas.

BIBLIOGRAPHY

1. S. Silver, *Microwave Antenna Theory and Design,* London: P. Peregrinus, 1984.

2. A. D. Oliver et al., *Microwave Horns and Feeds,* London: P. Peregrinus, 1994.

3. Y. T. Lo and S. W. Lee, *Antenna Handbook, Theory Applications and Design,* New York: Van Nostrand Reinhold, 1988, chap. 16.

4. R. C. Johnson and H. Jasik, *Antenna Engineering Handbook,* 2nd ed., New York: McGraw-Hill, 1984.

5. M. Barakat and L. Shafai, Studies on certain modified Luneberg lenses, *IEE Proc.,* **130**, part H (5): 363–368, 1983.

6. G. Bekefi and G. W. Farnell, A homogeneous dielectric sphere as a microwave lens, *Can. J. Phys.,* **34**: 790–803, 1956.

7. V. B. Mason, The electromagnetic radiation from simple sources in the presence of a homogeneous dielectric sphere, PhD dissertation, Univ. of Michigan, 1972.

8. P. J. B. Clarricoats, A. D. Oliver, and M. Rizk, A dielectric loaded conical feed with low cross-polar radiation, *Proc. URSI Symp. EM Theory,* Spain, 1983, pp. 351–354.

9. E. Lier, A dielectric hybrid mode antenna feed, a simple alternative to the corrugated horn, *IEEE Trans. Antennas Propag.,* **AP-34**: 21–29, 1986.

10. R. W. P. King et al., The insulated monopole: Admittance and junction affect, *IEEE Trans. Antennas Propag.,* **AP-23**: 172–177, 1975.

11. I. J. Bahl and S. S. Stuchly, Analysis of a microstrip covered with a lossy dielectric, *IEEE Trans. Microw. Theory Tech.,* **MTT-28**: 104–109, 1980.

L. SHAFAI
University of Manitoba